Predicting Spread of Alzheimer's Disease Pathology Using Brain Connectomes from Different Cognitive Stages

1. Introduction

Alzheimer's disease (AD) has long been the most common cause of dementia [3]. In 2021, it was estimated that 57 million people were living with dementia already, and the number is expected to increase by 10 million each year [30]. However, the exact mechanism and spread of the disease are still not fully understood [12].

Past studies have revealed that accumulation of amyloid-beta and tau proteins has a crucial role in the development of AD. The former one as plaques and the latter one as tangles, both proteins accumulate as the disease progresses. A popular research framework proposed by the National Institute on Ageing and Alzheimer's Association (NIA-AA) is the AT(N) framework [11], which integrates studies in amyloid-beta (A), tau (T), and neurodegeneration (N). Under this framework, in vivo neuroimaging techniques such as positron emission tomography (PET) and magnetic resonance imaging (MRI) are used to identify the presence of pathology hallmarks [13]. In this report, this work mainly focuses on the PET images of tau supplemented by amyloid-beta distribution, which has been shown to be a reliable way to identify the presence of amyloid and tau pathology [9].

Contemporary views suggest that tau pathology does not spread in a cell-autonomous manner like independent events, but rather affected by factors external to cells [8]. One of these factors recently studied is the brain connectome. A hypothesis to explain the characteristic spread of tau pathology is that the rate of spread is affected by how strongly brain regions connect [28]. Tau proteins may spread through synapses, when neurotransmitters are passed.

In brain connectomes, neural elements (e.g. neurons, gray matter) serve as nodes, and their connections or interactions (e.g. axons, functional annotations) define edges [26]. Reproducible findings have highlighted that human brains are small-world [2] (high clustering and short path), rich-club [23, 24] (denser connections between high degree nodes), and hierarchically modular [15, 20] (composed of subnetworks) networks. However, the brain connectomes, both structurally and functionally, change with disease progression [31], making it challenging to model with static connectome.

This project aims to explore how tau pathology spread over time, at different brain regions, and at different cognitive states. Connectome properties at different stages of the disease are compared, as well as three models to predict tau accumulation. The latter is done in a probabilistic view considering performance and complexity. Finally, the models are benchmarked against null models to validate the effect of connectome topology and amyloid-beta weights on the predictions.

2. Methods

2.1. Dataset

The dataset used in this project is structural connectomes from Dr Oxtoby [16] and PET images of amyloid and tau from the Alzheimer's Disease Neuroimaging Initiative (ADNI) database. Structural connectomes from 4 stages of Alzheimer's disease (AD) are available:

- Cognitively normal (CN)
- Early mild cognitive impairment (EMCI)
- Late mild cognitive impairment (LMCI)
- Probable Alzheimer's disease (DEM)

Each cognitive state has 42 participants connectomes, and each connectome is constructed from 84 regions of interest (ROIs). The connectomes are undirected, positively weighted graphs, where the nodes are the ROIs and the edges are assumed to be fully connected but weighted. More formally, each connectome matrix $m \in \mathbb{R}^{84\times84}$, where $m_{ij} = m_{ji}$, $m_{ii} = 0$, and $m_{ij} \geq 0$.

Two PET image data from ADNI are used as well, one for tau and another one for amyloid-beta. Both proteins are measured in standard uptake value ratio (SUVR), across all 84 regions. The data collection and procedure are described in ADNI PET Processing Methods protocol [14]. Among them, the tau PET image is used as the target for prediction, and the amyloid-beta PET image is used in one of the models. Subcortical regions were not included in the predictions, since they are affected by off-target binding, when

the tau-PET tracer misidentifies other structures as tau proteins. Only 68 ROIs were used in the actual predictions. The region labels and order is given by Raj et al.'s list [17].

2.2. Connectome Properties

To calculate and investigate connectome properties of different cognitive states, this project used Brain Connectivity Toolbox (BCT) library and the measures listed in Bullmore and Sporns' work [4]. After reviewing the literature, 5 connectome properties were selected to be compared across cognitive stages, to see how they change as the disease progresses. These were:

- Node degree: the number of edges connected to a node, which is a measure of the connectivity of a node.
- Clustering coefficient: fraction of neighbours of a node that are connected to each other.
- Global efficiency: the inverse of the average shortest path length in the network, which is a measure of how efficiently information can be transmitted through the network.
- Rich-club coefficient: measure of how unexpectedly and densely connected the high degree nodes are among themselves.
- Betweenness: fraction of shortest paths that pass through a given node, also a centrality measure related to hubness.

Yu et al. [31] provided a good overview of how these properties may be affected by the disease. The three former metrics were found to negatively correlate with the accumulation of amyloid-beta as AD progresses in previous studies [31]. For example, although AD is seen as "disconnection syndrome" [31], gray matter volume was not observed to decrease; instead, nodal degree of gray matter and small-worldness are reduced [21]. The progression also lowers global efficiency [27] and the clustering coefficient because of lower connectivity [25]. The rich-club coefficient is a characteristic of human brain connectome, so it would be interesting to see how it changes as the disease progresses. The betweenness centrality is also affected by by amyloid-beta accumulation in some cases [31].

2.3. Models

Spreading models used in this work are implemented using the Network Spreading Models (NSM) toolbox [22]. The first Network Diffusion Model (NDM) is a base model that diffuses tau pathology at a rate dependent only on connectome weights [17]. The rate of spread is defined as Equation 1, where $\tau(t)$ is the tau concentration at time t, β is the diffusion constant, and H is the Laplacian of the connectome.

$$\frac{d\tau(t)}{dt} = -\beta \cdot H \cdot \tau(t) \tag{1}$$

However, NDM doesn't take the natural production of tau in brain regions in to account, thus a new model was proposed, the Fisher-Kolmogorov-Petrovsky-Piskunov (FKPP) model [29]. This version adds local production of tau, defined as Equation 2, where α is the weight given to the spread contribution as opposed to the local production. The new part of the expression $(1-\alpha)\cdot\tau(t)\cdot(1-\tau(t))$ is a logistic growth term, which simulates population growth in a limited environment (tau can't be reproduced indefinitely).

$$\frac{d\tau(t)}{dt} = -\alpha \cdot H \cdot \tau(t) + (1-\alpha)\cdot\tau(t)\cdot(1-\tau(t)) \tag{2}$$

Despite adding self-production in FKPP, this model introduces it in a uniform production rate. The third model, Weighted FKPP improves upon this by considering the external factors influencing the rate of self-production. In this work, the self-production rate of tau is weighted by the amyloid-beta pathology in the same region, as these two often correlate in AD. Equation 3 shows the new model, where $\mathbf{v}$ is the weights vector, which is chosen to be amyloid-beta concentrations.

$$\frac{d\tau(t)}{dt} = -\alpha \cdot H \cdot \tau(t) + \mathbf{v}\cdot(1-\alpha)\cdot\tau(t)\cdot(1-\tau(t)) \tag{3}$$

Finally, reproducibility is ensured by setting a fixed random seed on stochastic processes such as permutation and rewiring.

3. Results

3.1. Core Tasks

3.1.1 Connectome Properties across Cognitive Stages

42 connectomes for each of the 4 cognitive stages are loaded as 84×84 matrices. The strength of connections between regions is visualised as a heatmap, as shown in Figure 1. Most regions have weak connections, except for a few pairs. In this example (subject 0 in CN state), the strongest connection occurs between `Superiorparietal_R` and `Precuneus_R`.

To compare across stages, 42 connectomes are first normalised to $[0, 1]$ range, and then the BCT library, 5 properties are calculated. Except for the global efficiency, all other properties are averaged across regions within each connectome. The rich-club coefficient requires additional thresholding, binary conversion, and `nan` handling to compute.

With the list of 5 connectome properties of each group, a Kruskal-Wallis statistical test is performed to see if the distributions of the properties are significantly different across

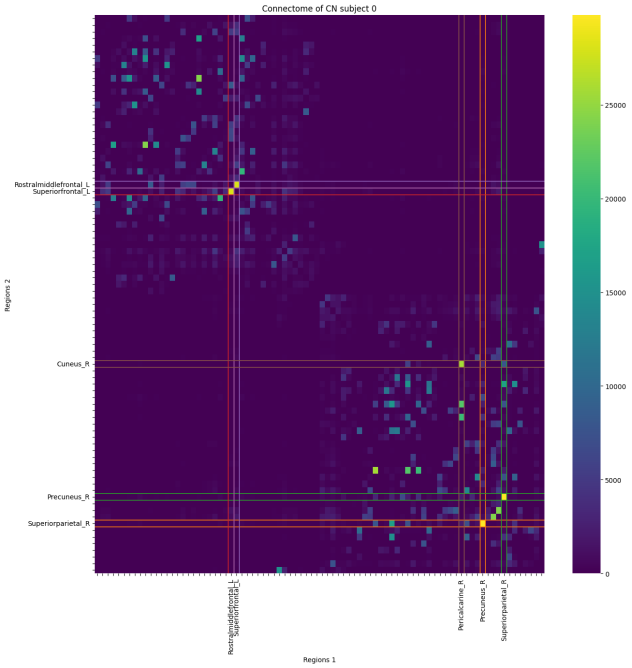

Figure 1. Example heatmap of the connectome strength for the CN stage for subject 0. The top 5 strongest connections are highlighted. Region label sizes are kept small to correspond to each of the 84 regions.

Property	Statistic	P-value	Significance
Degree	2.0659	0.5588	Not significant
Clustering Coefficient	8.1969	0.0421	Significant
Global Efficiency	12.0281	0.0073	Significant
Rich Club	2.9428	0.4005	Not significant
Betweenness	1.5656	0.6672	Not significant

Table 1. Kruskal-Wallis test results for different cognitive groups. Metrics with P-values below 0.05 are considered significant.

groups. This non-parametric test was chosen to relax the normality assumption and ensure robustness against outliers. The results are shown in Table 1.

Clustering coefficient and global efficiency were found to be significantly different across groups, but Kruskal-Wallis test does not indicate which pairs of groups are significantly different. Thus, a post-hoc Dunn's test was performed using `scikit_posthocs` library, to analyse each pair of groups. The results are shown in Table 2. Bonferroni adjustment was applied due to its straightforwardness and conservative approach for p-value adjustment. The results of all properties across cognitive groups are illustrated in Figure 2. Clustering coefficient and global efficiency are found to be significantly different across CN and DEM groups only, both reduced in DEM state. Clustering

Clustering Coefficient	CN	EMCI	LMCI	DEM
CN	1.0000	0.2500	1.0000	**0.0391**
EMCI	0.2500	1.0000	1.0000	1.0000
LMCI	1.0000	1.0000	1.0000	0.8253
DEM	**0.0391**	1.0000	0.8253	1.0000
Global Efficiency	CN	EMCI	LMCI	DEM
CN	1.0000	0.1138	0.3207	**0.0043**
EMCI	0.1138	1.0000	1.0000	1.0000
LMCI	0.3207	1.0000	1.0000	0.8764
DEM	**0.0043**	1.0000	0.8764	1.0000

Table 2. Dunn's test results for Clustering Coefficient and Global Efficiency. Pairwise P-values are shown comparing groups CN, DEM, EMCI, and LMCI.

coefficients differed significantly at the 0.05 level, whereas global efficiency differed even more at the 0.01 level. No other pairs of groups at any property were found to be significantly different.

3.1.2 NDM and FKPP Modelling

Next, tau accumulation is modelled using NDM and FKPP models. These models accept a single connectome, target tau data, and a region list of interest (68 regions in this case). The target tau data is the tau PET image, min-max normalised to $[0, 1]$ range, of 68 selected regions. Single connectomes are obtained for each of the four cognitive states, aggregated by first min-max normalising and then averaged. The resulting connectomes are shown in Figure 3, where differences are subtle.

Inside the Network Spreading Models toolbox, each region is explored at a time to be the epicentre and model its propagation over time. After finding the time point that best explains target tau distribution, the lowest SSE (sum of squared errors) seed is selected.

For both models, the optimal seed, ideal time index, SSE, and Pearson's Correlation were recorded as shown in Table 3. For all four cognitive states, the spread over time and prediction correlation are shown in Figure 4.

The first observation is that predictions are quite consistent across cognitive states, with similar optimal time points and the same epicentre: inferior temporal cortex. Despite the same epicentre, the optimal time point, i.e. the predicted time the target tau data was collected, is sooner in NDM (around 42) than FKPP (around 82). It can also be observed that NDM's prediction tends to align more closely with the target tau data than FKPP. However, lower SSE in FKPP indicates that FKPP is closer to predictions than NDM at certain points. Finally, for example CN (similar for other states), the spread of tau in different regions shows FKPP

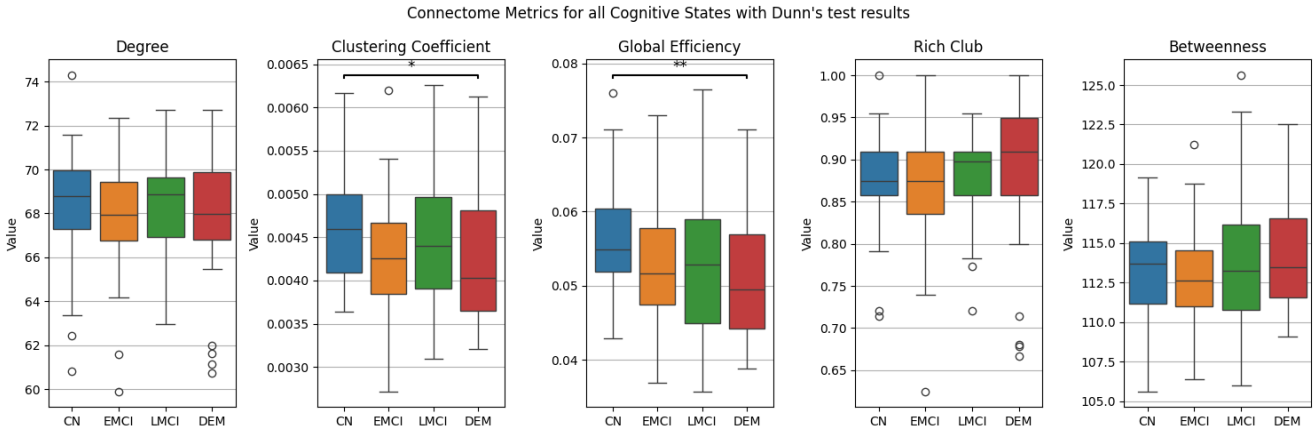

Figure 2. Dunn's test results for all 5 connectome properties across cognitive groups. P-values thresholds are: * = 0.05 and ** = 0.01.

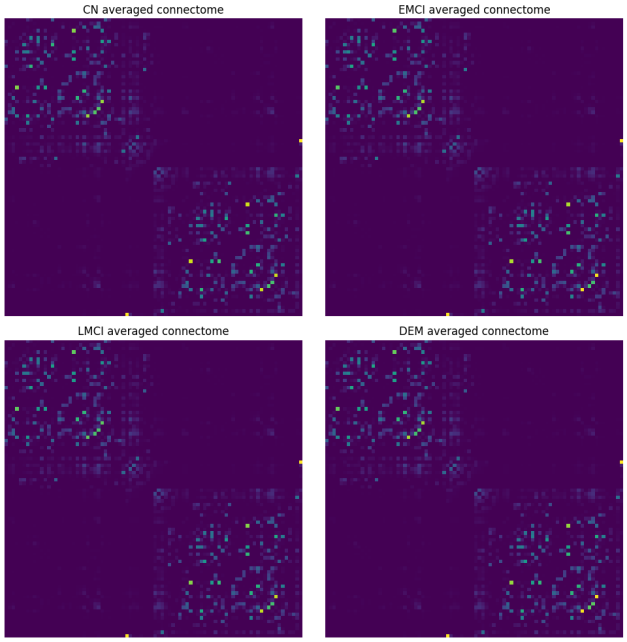

Figure 3. Average connectome of the four cognitive states.

having a noticeable downwards curve at the beginning compared to NDM. More interpretation is deferred to discussion section.

To better compare the models taking complexity into account, corrected Akaike Information Criterion (AICc) is calculated for both models at each cognitive state. For NDM, the degree of freedom is set to be 2 (seed and diffusion constant), and for FKPP 3 (extra for logistic growth rate). Seed region is considered to be 1 instead of 68 since the fitting process is done for each region separately. The resulting AICc and weights are shown in Figure 5. For all cognitive states, FKPP model is preferred over NDM by a large margin. This suggests that while FKPP is more complex, the explanatory power it provides is worth the extra complexity.

NDM	Seed	Timepoint	SSE	r
CN	Inferiortemporal	43	2.4837	0.7244
EMCI	Inferiortemporal	42	2.5316	0.7188
LMCI	Inferiortemporal	41	2.6184	0.7180
DEM	Inferiortemporal	43	2.5648	0.7143
FKPP	Seed	Timepoint	SSE	r
CN	Inferiortemporal	82	2.2669	0.6492
EMCI	Inferiortemporal	82	2.3105	0.6416
LMCI	Inferiortemporal	81	2.3418	0.6395
DEM	Inferiortemporal	82	2.3283	0.6402

Table 3. Results for best-fit NDM and FKPP models based on average cognitive connectomes.

Further comparison can be done using Enigma Toolbox to visualise the residuals of the models. The residuals are calculated as the difference between target tau data and predicted tau data. Then, as cognitive states show ver similar residual map within the same model, only DEM state is selected to visualise residuals as brain region heatmap, for both NDM and FKPP models. This is shown in Figure 6. The residuals of both models show similar patterns, with more intense residuals in lateral regions than medial regions. The parietal and temporal lobe are mostly negative residuals whereas frontal and occipital cortex are mostly positive. The medial temporal lobe, where seeds normally reside, has barely residuals, it may have indicated both models' good prediction, but it could also due to the removal of subcortical regions in the predictions. In contrast, they differ in that FKPP has noticeable smaller residuals in frontal parietal regions, and overall, the residuals are less intense

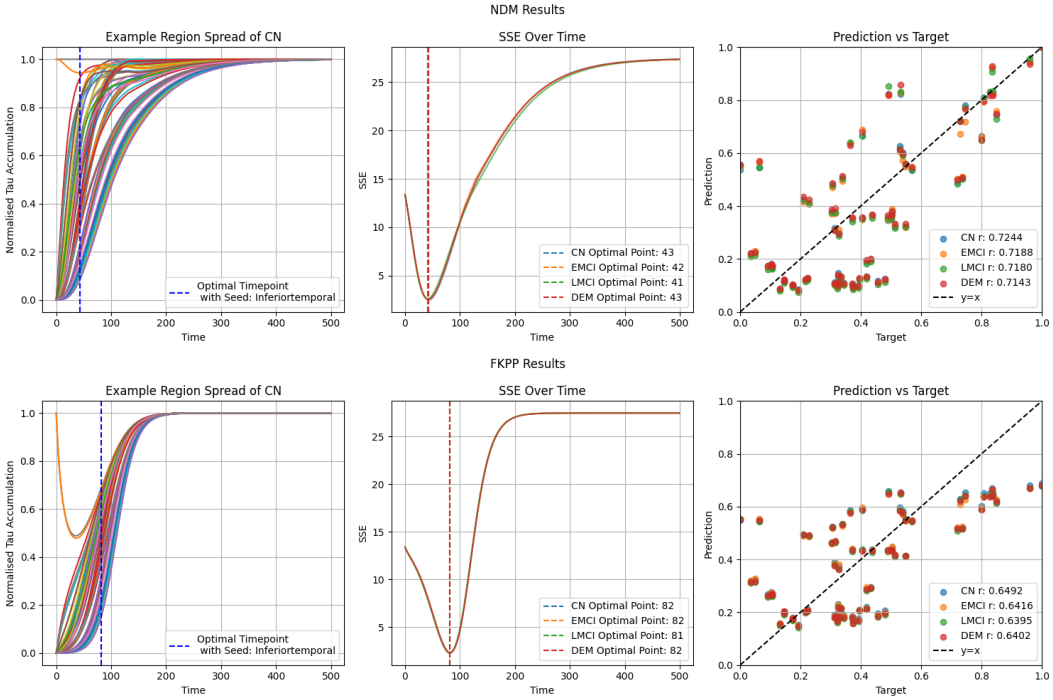

Figure 4. NDM and FKPP models results for all four cognitive states. The left column shows an example of region spread for CN stage. The centre column shows the SSE of predictions at different time points. The right column shows the scatter plot of prediction vs target tau values.

along superior regions.

Despite average connectome gives an aggregated view of the connectome, it is not able to capture the individual differences. To visualise the tendency of participant-wise predictions, individual level connectomes are fitted with NDM and FKPP models. To speed up FKPP fitting which can take hours to run, candidate seed region were reduced from 68 to 6 regions {`Inferiortemporal`, `Temporalpole`, `Amygdala`, `Entorhinal`, `Hippocampus`, `Middletemporal`}. The selection criteria is based on top 5 regions with lowest SSE for any cognitive state from NDM. In the meanwhile, the full list is not available for FKPP unfortunately. Only 6 regions were selected, as the best seed regions across cognitive states are highly similar and likely to reside in this small subset. The number of calls and initial points in FKPP were also halved from 200 and 128 to 100 and 64 respectively.

The distribution of Pearson's correlation, SSE, and optimal seed regions are shown in Figure 7. From Pearson's correlation distribution, it can be seen that NDM has two separated peaks, whereas FKPP has a single peak somewhere in the middle. This indicates that NDM is better at predicting for a big subset of participants, but performs worse for remaining participants. FKPP tends to predict more consistently across participants. The SSE distribution shape is similar, but FKPP has overall lower SSE, which is reasonable since it is a more complex model. Finally, the seed regions in FKPP are less diverse compared to NDM, but this could be due to the smaller pool of candidate regions.

Weighted FKPP	Seed	Timepoint	SSE	r
CN	Entorhinal	81	1.8519	0.7198
EMCI	Entorhinal	81	1.8837	0.7141
LMCI	Entorhinal	82	1.9273	0.7078
DEM	Entorhinal	82	1.9082	0.7110

Table 4. Results for best fitted Weighted FKPP (weighted by amyloid-beta accumulation) models based on average cognitive connectomes.

3.2. Advanced Tasks

3.2.1 Amyloid-beta Weighted FKPP Modelling

Accumulation of amyloid-beta could be indicative of the tau pathology spread, so it is investigated by adding it as weights to the Weighted FKPP model. The same procedure of min-max normalisation and averaging is followed as in FKPP, but this time setting weights to the amyloid-beta concentrations in the same region.

The results of best-fitted Weighted FKPP are shown in

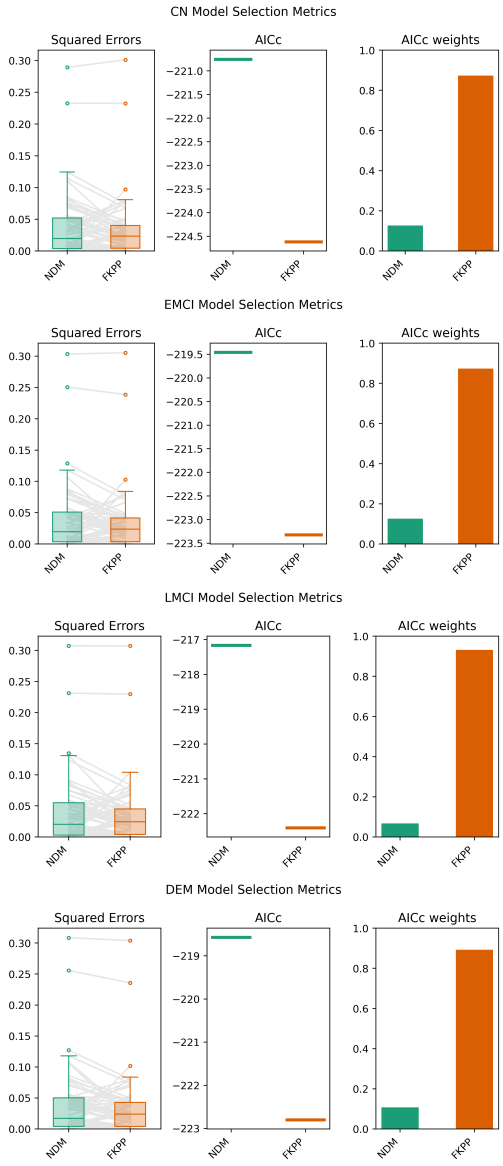

Figure 5. AICc for NDM and FKPP models at each cognitive state. The lower the AICc and higher AICc weights, the better the model.

Table 4. The optimal seed now appears to be `Entorhinal` instead of `Inferiortemporal`. The time point remains similar to FKPP, with r approaching NDM, while SSE is much lower than both NDM and FKPP, indicating superior fit. When taking the complexity into account, AICc of all three models is shown in Figure 8. The degrees of freedom is set to 4 for Weighted FKPP, considering amyloid-beta weights to be another parameter. As observed, Weighted FKPP is still preferred over FKPP and NDM even with the extra complexity, and the difference surpasses that of FKPP compared to NDM. This remains consistent across cognitive states. In summary, amyloid-beta Weighted FKPP better predicted tau spread, as supported by AICc weights.

Another experiment worth analysing is the comparison of Weighted FKPP and non-weighted FKPP under the same set of parameters, the best ones found by Weighted FKPP. By setting optimal seed, time point, and diffusion constant to the ones found by Weighted FKPP, a new FKPP model was fitted. Then, the difference in predictions between the two models are calculated with $\text{Weighted FKPP prediction} - \text{FKPP prediction}$, resulting in Figure 9. Since all cognitive states look similar, only DEM state is thus shown. The residuals are mostly positive, being stronger in frontal regions and weaker in the parietal-occipital cortex, which complements the underprediction of FKPP in these regions. No differences in medial temporal lobe or subcortical regions again.

3.2.2 Null Model Benchmarking

Null modelling is often used to validate the results of a model. In the brain network context, this means randomisation and permutation of some characteristics in the model, while maintaining the rest [26]. The null hypothesis is that the model's outcome, using r values in this work, is not significantly different from the null model, given that randomised characteristics are not the cause of the outcome. With many randomisations, the r values from null models can be used to create a distribution, the null distribution. Then, the original r value can be compared to the null distribution to see if it is significantly different, i.e. empirical p-value relative to the significance level.

The first property to benchmark is incorporation of amyloid-beta. The null hypothesis would be that amyloid-beta weights in the same region do not affect the performance of Weighted FKPP. To obtain null models, the original amyloid-beta for different regions is permuted, so that the weights are retained but in different positions. After fitting, the Pearson's r values are recorded. This process is repeated 1000 times to ensure robustness, which is evidenced by the stability of p-values with respect to permutation number in Figure 10, for all cognitive states. To speed up the process of 1000 Weighted FKPP fitting, the number of calls was reduced from 200 to 50, and the number of initial points from 128 to 32. Tests on 10 samples showed that this reduction did not significantly affect the results. Adding on to the parallel processing with `joblib` library and 20 CPU cores, each run were reduced from about half an hour to five seconds on average.

The resulting p-values for each cognitive state and their null distribution are shown in Figure 12. It can be seen that original amyloid-beta weights resulted in an r value that is significantly different from the null distribution. The significance level of all cognitive states are below 0.05, with EMCI, LMCI, and DEM being below 0.01. This rejects the

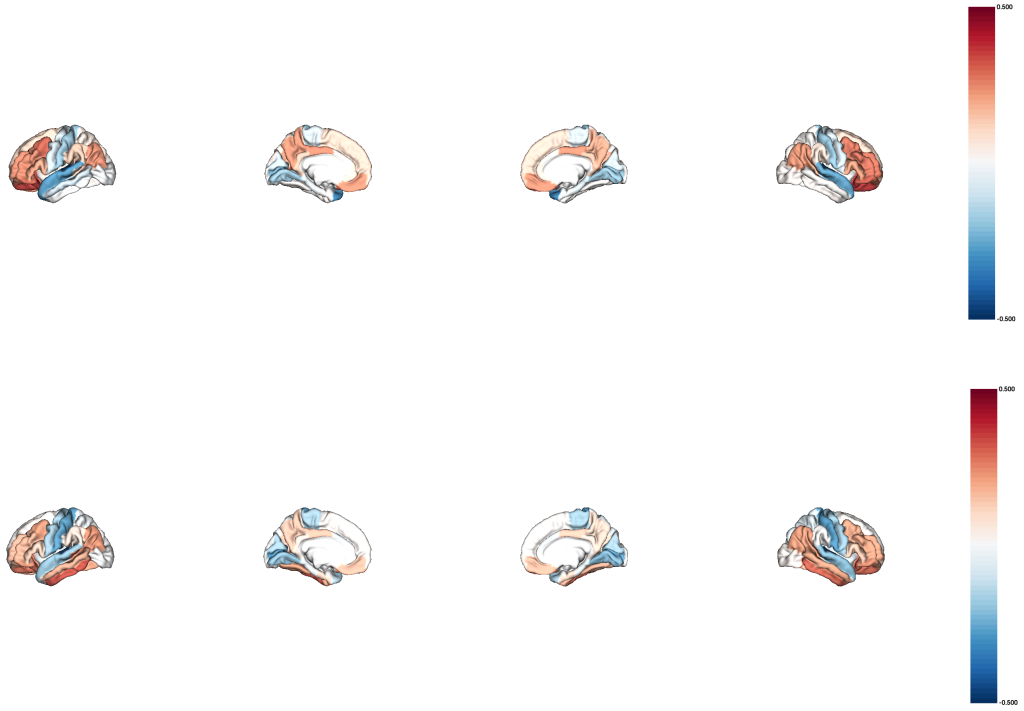

Figure 6. Cortical residuals of NDM (top) and FKPP (bottom) models for DEM stage. The residual is calculated with $\text{target} - \text{prediction}$. The colour bar indicates the value of the residuals, where red indicates positive residuals and blue indicates negative residuals.

null and verifies that increase in performance observed in Weighted FKPP is not due to random chance, but rather the incorporation of valid amyloid-beta weights.

Another property worth benchmarking is the topology of the connectome. The connection weights among regions are intuitively not trivial. Thus, to test the null hypothesis that the topology of the connectome does not affect the model's performance, rewiring is done to randomise the weights. The rewiring process is done by randomly selecting a pair of edges and swapping their endpoints, in this case, the weights [26]. This process is implemented using BCT library's `null_model_und_sign` function, to ensure degree, weights, and in- and out- strength distributions are maintained in the connectome. Such rewiring is conducted on the best performing average connectome, CN state, for its lowest SSE and highest r. Null benchmarking is performed on all three models, NDM, FKPP, and Weighted FKPP, each with 1000 rewirings.

The stability of the p-values with respect to the number of rewirings is shown in Figure 11. Interestingly, the p-values of all three models on CN state reached the 0.001 significance level after 1000 rewiring, indicating that the original r value is significantly different from all conducted rewirings. This if further supported by the distribution of the null models in Figure 13. The original r value was the highest among all rewired r values and in all models. This strongly rejects the null suggesting that the topology of the connectome does indeed strongly affect the performance of the model.

4. Discussion

4.1. Connectome Analysis

Connectome across cognitive states surprisingly didn't have a significant difference on degree, rich-club, and betweenness centrality. One possible reason and caveat is that each connectome's properties are averaged across regions, which may obscure the characteristics of the stages. For example, the degree of a specific region may be significantly different across stages, but the average degree across all regions might fail to show a significant difference.

Significant decrease in clustering coefficient and global efficiency in DEM stage is consistent with previous studies [27, 31]. This is a sign that at dementia stage, the brain connectome indeed loses its local connections (clustering coefficient) and the ability to transmit information efficiently across the brain (global efficiency). Thus AD is sometimes suggested as "disconnection syndrome" [5, 6].

When modelling with average connectomes, this caveat should also be kept in mind. In fact individual level connec-

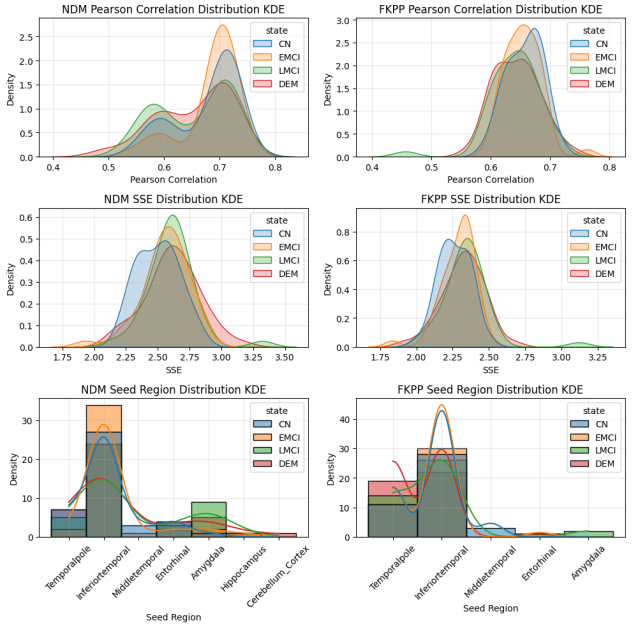

Figure 7. Individual level NDM and FKPP models results distribution for all four cognitive states. Density plots of Pearson's correlation, SSE, and optimal seed region are shown.

tomes are usually different, but the averaged connectome looks similar in all cognitive states, which may obscure precision in subsequent spread modelling.

4.2. NDM, FKPP, and the Need for Weighted FKPP

Consistent spread across cognitive groups in NDM and FKPP probably indicates it achieves similar modelling performance across different stages. But it could also be due to insufficient distinction between connectomes.

From time point of view, FKPP predicted the tau to be in a later stage in time than NDM, which means that introducing self-production in the loop takes longer for tau to achieve target tau level. Region spread further proves the point; more time is needed to reach the optimal time point, initial downwards trend indicate less accumulation in seed compared to other regions. But once passed this point, the curve's ascent is steeper (quicker) than NDM. Also, introducing self-production increases homogeneity, lines representing regions are more similar, as opposed to NDM which has large fluctuations depending on the region.

Optimal seed of inferior temporal was explored in a previous fMRI-PET study [7], where strong tau covariance was observed in this region. Another findings suggests that tau concentration in inferior temporal may correlate with amyloid-beta accumulation, rather than cognitive impairment [19]. However, a further study reported that tau accumulation in inferior temporal was linked to hippocampal activity but not amyloid-beta accumulation [10]. So, inferior temporal lobe is a controversial region for tau epicentre in the literature.

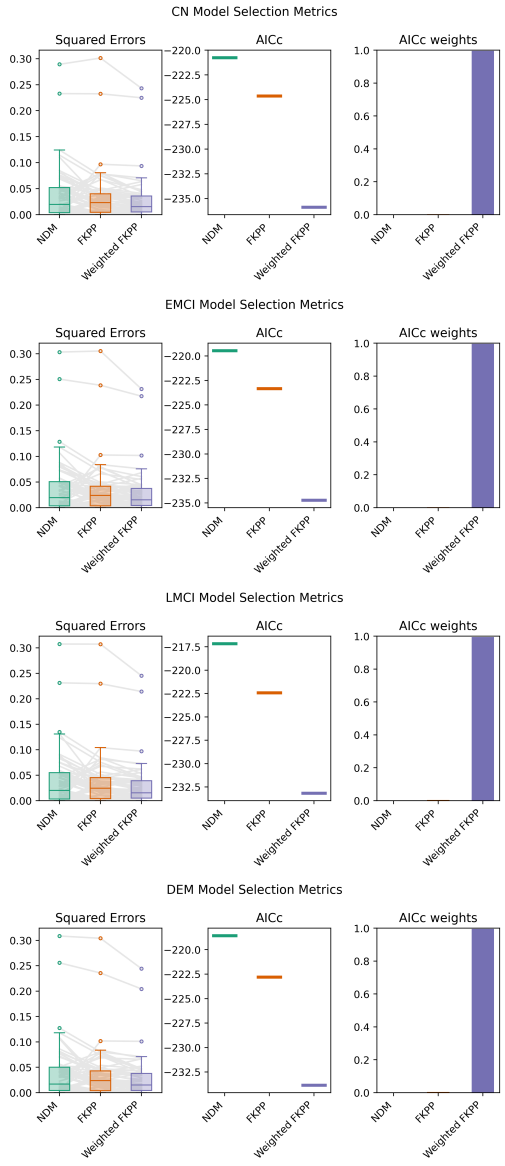

Figure 8. AICc for NDM, FKPP, and Weighted FKPP models at each cognitive state. The lower the AICc, the better the model, with higher AICc weights indicating preference.

When comparing residuals in NDM and FKPP models prediction, they both showed uneven pattern. Since residual are calculated by $\mathrm{target} - \mathrm{prediction}$, blue regions indicate that models are over predicting in temporal and parietal regions, putting too much emphasis. The lack of coloured residuals in medial temporal regions, may seem to suggest accurate predictions, but it is probably due to removal of subcortical regions in prediction. Whereas underprediction in frontal and occipital regions indicate the need for an ad-

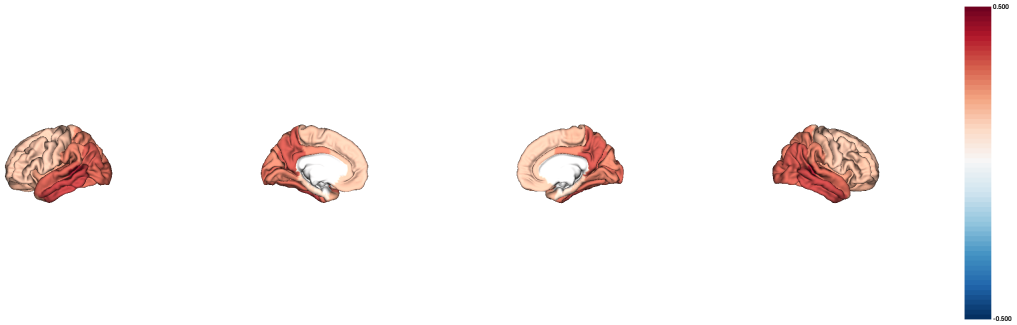

Figure 9. Cortical residuals between Weighted FKPP and non-weighted FKPP under best parameters of Weighted FKPP, for DEM stage. The residual was calculated with Weighted FKPP prediction − FKPP prediction. The colour bar indicates the value of the residuals, where red represents positive residuals and blue negative residuals.

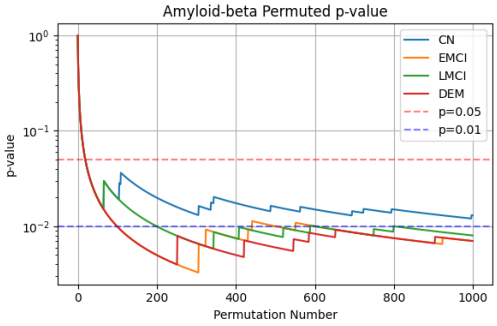

Figure 10. P-value of original r value compared to null distribution by permuting amyloid-beta weights. Weighted FKPP model for four cognitive states. The plot stabilises after 1000 permutations for all cognitive groups.

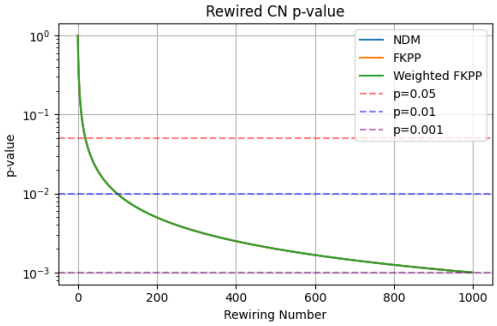

Figure 11. P-value of original r value compared to null distribution by rewiring the connectome. All three models predicting on CN state. Only one line is visible because the trends are identical and the lines overlap.

ditional factor to regulate their acceleration. This underprediction is less pronounced in FKPP perhaps because it incorporates self-production and does not entirely rely on spread.

Individual level plots showed that Pearson's correlation is generally higher in earlier stages of disease, e.g. CN or EMCI, which may be indicative of easier modelling. The small group in CN that shifted to lower SSE in both plots may be due to the fact that CN's connectomes are more typical and less changed by the disease. As the disease progresses, as mentioned earlier, the structure of the connectome may be affected, which increases the complexity of the modelling progressively. However this is not reflected with any external factor in NDM and FKPP models. Thus, there is a need for more complex models like Weighted FKPP.

Weighted FKPP also was consistent in optimal seed region across cognitive states, although switching from inferior temporal to the entorhinal cortex. Previous findings also identified the entorhinal cortex as one of the initial epicentre of tau spread in AD [1, 18]. The time point similar to FKPP indicates they predict tau to roughly propagate at the same speed, but when regulated with amyloid, the fit was significantly better, with substantial lower SSE.

The AICc weights with all three model showed that Weighted FKPP is preferred over FKPP over NDM. This finding is a sign that the extra complexity in developing these new models is worthwhile, as they are able to explain the data better by adding parameters in an effective way.

Enigma visualisation of differences in prediction between Weighted FKPP and non-weighted FKPP of the same parameters, indicate that tau accumulation in lateral temporal lobe is boosted. This is exactly what the previous models were failing, by underpredicting these areas. So, providing amyloid-beta weights to the model better accounts for the extra tau accumulation in these regions. Finally, no differences in medial temporal regions are expected due to subcortical regions removal.

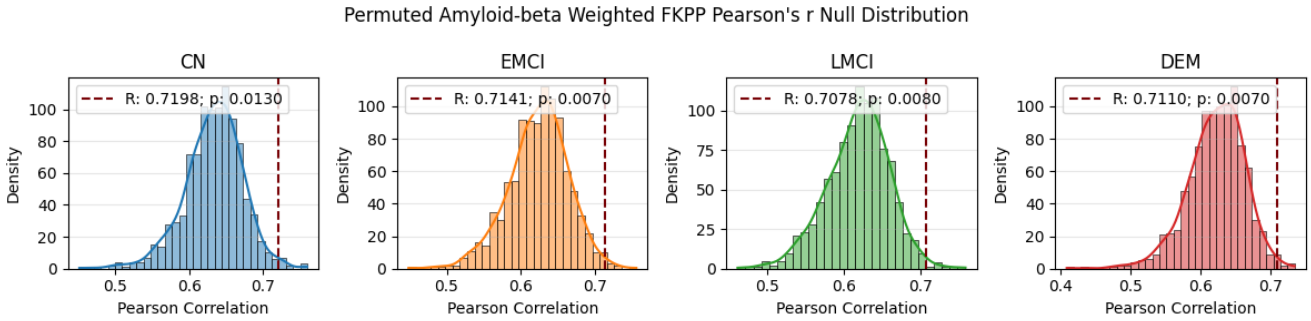

Figure 12. P-value of original r value compared to null distribution of 1000 permutations of amyloid-beta weights, for all cognitive groups.

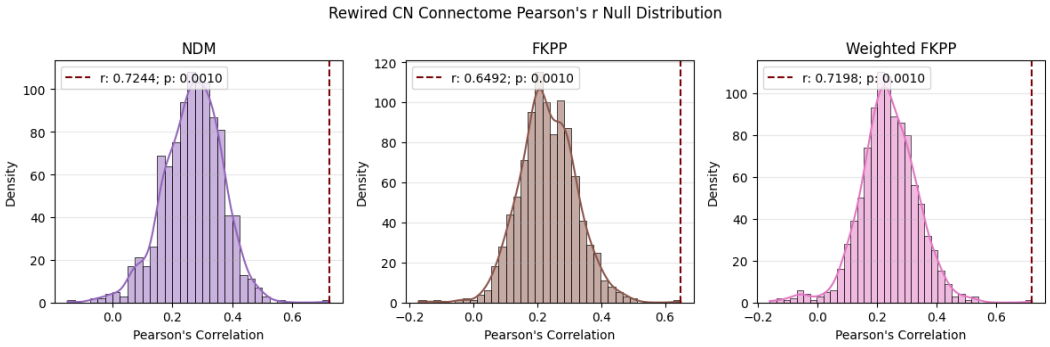

Figure 13. P-value of original r value compared to null distribution of 1000 rewiring of the CN connectome, for all three models.

4.3. Verified Effect of Factors on Tau Spread

For amyloid-beta null benchmarking, the p-values were all below 0.05 for all cognitive states and below 0.01 for most of them, indicating the importance of incorporating proper weights in the model. Rejection of null hypothesis also further supports the idea that more accurate prediction of tau pathology is indeed influenced by amyloid-beta accumulation in the same region, and not just by random chance.

Strong rejection at 0.001 significance level for topology rewiring indicates that the connectome topology is ultimately important for all three models to predict tau spread. This appears to be even more relevant than the weights of amyloid-beta, since amyloid-beta permutation do get higher r by random chance, but none in these 1000 topology rewirings. This strongly supports the idea of tau spread is modelled by connectome factors [28].

5. Conclusion

This project explored connectome properties and different models of tau spread in progressive stage from healthy to AD. From calculated properties, clustering coefficient and global efficiency were found significantly different between CN and DEM stages, suggesting disconnections in the brain. The three models of tau spread, NDM, FKPP, and Weighted FKPP were compared, in the order of increasing complexity and accuracy. Conducting AICc analysis, Weighted FKPP was preferred over FKPP and NDM, even with the extra complexity. The need for extra regulating weights such as amyloid-beta was suggested by exploring residuals and individual-level fittings. Finally, the null benchmarking confirmed the importance of both amyloid-beta weights and connectome topology in the modelling process.

References

[1] Jenna N Adams, Anne Maass, Theresa M Harrison, Suzanne L Baker, and William J Jagust. Cortical tau deposition follows patterns of entorhinal functional connectivity in aging. *elife*, 8:e49132, 2019. 9

[2] Danielle S Bassett and Edward T Bullmore. Small-world brain networks revisited. *The Neuroscientist*, 23(5):499–516, 2017. 1

[3] Indu Bhushan, Manjot Kour, Guneet Kour, Shriya Gupta, Supriya Sharma, and Arvind Yadav. Alzheimer's disease: Causes & treatment–a review. *Ann Biotechnol*, 1(1):1002, 2018. 1

[4] Ed Bullmore and Olaf Sporns. Complex brain networks: graph theoretical analysis of structural and functional systems. *Nature reviews neuroscience*, 10(3):186–198, 2009. 2

[5] Marco Catani and Dominic H Ffytche. The rises and falls of disconnection syndromes. *Brain*, 128(10):2224–2239, 2005. 7

[6] Xavier Delbeuck, Martial Van der Linden, and Fabienne Collette. Alzheimer'disease as a disconnection syndrome? *Neuropsychology review*, 13:79–92, 2003. 7

[7] Nicolai Franzmeier, Anna Rubinski, Julia Neitzel, Yeshin Kim, Alexander Damm, Duk L Na, Hee Jin Kim, Chul Hyoung Lyoo, Hana Cho, Sofia Finsterwalder, et al. Functional connectivity associated with tau levels in ageing, alzheimer's, and small vessel disease. *Brain*, 142(4):1093–1107, 2019. 8

[8] Michel Goedert. Alzheimer's and parkinson's diseases: The prion concept in relation to assembled aβ, tau, and α-synuclein. *Science*, 349(6248):1255555, 2015. 1

[9] Oskar Hansson. Biomarkers for neurodegenerative diseases. *Nature medicine*, 27(6):954–963, 2021. 1

[10] Willem Huijbers, Aaron P Schultz, Kathryn V Papp, Molly R LaPoint, Bernard Hanseeuw, Jasmeer P Chhatwal, Trey Hedden, Keith A Johnson, and Reisa A Sperling. Tau accumulation in clinically normal older adults is associated with hippocampal hyperactivity. *Journal of Neuroscience*, 39(3):548–556, 2019. 8

[11] Clifford R Jack Jr, David A Bennett, Kaj Blennow, Maria C Carrillo, Billy Dunn, Samantha Budd Haeberlein, David M Holtzman, William Jagust, Frank Jessen, Jason Karlawish, et al. Nia-aa research framework: toward a biological definition of alzheimer's disease. *Alzheimer's & dementia*, 14(4):535–562, 2018. 1

[12] Bryan D James and David A Bennett. Causes and patterns of dementia: an update in the era of redefining alzheimer's disease. *Annual review of public health*, 40(1):65–84, 2019. 1

[13] Keith A Johnson, Nick C Fox, Reisa A Sperling, and William E Klunk. Brain imaging in alzheimer disease. *Cold Spring Harbor perspectives in medicine*, 2(4):a006213, 2012. 1

[14] JiaQie Lee, Tyler Ward, Theresa Harrison, Susan Landau, and William Jagust. *Tau PET Processing Methods, ADNI Database*, 2023. 1

[15] David Meunier, Renaud Lambiotte, and Edward T Bullmore. Modular and hierarchically modular organization of brain networks. *Frontiers in neuroscience*, 4:200, 2010. 1

[16] Neil P Oxtoby, Sara Garbarino, Nicholas C Firth, Jason D Warren, Jonathan M Schott, Daniel C Alexander, and Alzheimer's Disease Neuroimaging Initiative. Data-driven sequence of changes to anatomical brain connectivity in sporadic alzheimer's disease. *Frontiers in neurology*, 8:580, 2017. 1

[17] Ashish Raj, Amy Kuceyeski, and Michael Weiner. A network diffusion model of disease progression in dementia. *Neuron*, 73(6):1204–1215, 2012. 2

[18] Michael Schöll, Samuel N Lockhart, Daniel R Schonhaut, James P O'Neil, Mustafa Janabi, Rik Ossenkoppele, Suzanne L Baker, Jacob W Vogel, Jamie Faria, Henry D Schwimmer, et al. Pet imaging of tau deposition in the aging human brain. *Neuron*, 89(5):971–982, 2016. 9

[19] Aaron P Schultz, Jasmeer P Chhatwal, Trey Hedden, Elizabeth C Mormino, Bernard J Hanseeuw, Jorge Sepulcre, Willem Huijbers, Molly LaPoint, Rachel F Buckley, Keith A Johnson, et al. Phases of hyperconnectivity and hypoconnectivity in the default mode and salience networks track with amyloid and tau in clinically normal individuals. *Journal of Neuroscience*, 37(16):4323–4331, 2017. 8

[20] Olaf Sporns and Richard F Betzel. Modular brain networks. *Annual review of psychology*, 67(1):613–640, 2016. 1

[21] Mara Ten Kate, Pieter Jelle Visser, Hovagim Bakardjian, Frederik Barkhof, Sietske AM Sikkes, Wiesje M van Der Flier, Philip Scheltens, Harald Hampel, Marie-Odile Habert, Bruno Dubois, et al. Gray matter network disruptions and regional amyloid beta in cognitively normal adults. *Frontiers in aging neuroscience*, 10:67, 2018. 2

[22] Elinor Thompson, Anna Schroder, Tiantian He, Antoine Legouhy, Xin Zhao, James H Cole, Neil P Oxtoby, and Daniel C Alexander. Demonstration of an open-source toolbox for network spreading models: regional amyloid burden promotes tau production in alzheimer's disease. *Alzheimer's & Dementia*, 20:e093791, 2024. 2

[23] Martijn P Van Den Heuvel and Olaf Sporns. Rich-club organization of the human connectome. *Journal of Neuroscience*, 31(44):15775–15786, 2011. 1

[24] Martijn P Van den Heuvel and Olaf Sporns. Network hubs in the human brain. *Trends in cognitive sciences*, 17(12):683–696, 2013. 1

[25] Bernadette CM Van Wijk, Cornelis J Stam, and Andreas Daffertshofer. Comparing brain networks of different size and connectivity density using graph theory. *PloS one*, 5(10):e13701, 2010. 2

[26] František Váša and Bratislav Mišić. Null models in network neuroscience. *Nature Reviews Neuroscience*, 23(8):493–504, 2022. 1, 6, 7

[27] Olga Voevodskaya, Joana B Pereira, Giovanni Volpe, Olof Lindberg, Erik Stomrud, Danielle van Westen, Eric Westman, and Oskar Hansson. Altered structural network organization in cognitively normal individuals with amyloid pathology. *Neurobiology of aging*, 64:15–24, 2018. 2, 7

[28] Jacob W Vogel, Nick Corriveau-Lecavalier, Nicolai Franzmeier, Joana B Pereira, Jesse A Brown, Anne Maass, Hugo Botha, William W Seeley, Dani S Bassett, David T Jones, et al. Connectome-based modelling of neurodegenerative diseases: towards precision medicine and mechanistic insight. *Nature Reviews Neuroscience*, 24(10):620–639, 2023. 1, 10

[29] Johannes Weickenmeier, Mathias Jucker, Alain Goriely, and Ellen Kuhl. A physics-based model explains the prion-like features of neurodegeneration in alzheimer's disease, parkinson's disease, and amyotrophic lateral sclerosis. *Journal of the Mechanics and Physics of Solids*, 124:264–281, 2019. 2

[30] World Health Organization WHO. Demantia: Key facts. on, 2025. Accessed: 2025-04-07. 1

[31] Meichen Yu, Olaf Sporns, and Andrew J Saykin. The human connectome in alzheimer disease—relationship to biomarkers and genetics. *Nature Reviews Neurology*, 17(9):545–563, 2021. 1, 2, 7